

# Asymptotic Properties of an Autocorrelation Coefficient for Coherent Doppler Sonar

JEREMY DILLON AND LEN ZEDEL

*Memorial University of Newfoundland, St. John's, Newfoundland, Canada*

ALEX E. HAY

*Dalhousie University, Halifax, Nova Scotia, Canada*

(Manuscript received 27 September 2010, in final form 9 December 2010)

## ABSTRACT

A new formula is derived for the asymptotic form of the magnitude of an autocorrelation coefficient for coherent Doppler sonar. The autocorrelation magnitude is shown to be a biased estimator in the limit of infinite ensemble length. Numerical simulation of a Gaussian random process is used to verify the asymptotic formula and to show that a bias persists for finite pulse-pair averages. Validity of the asymptotic formula is also confirmed using a high-fidelity coherent Doppler sonar simulation, and from sonar measurements in a towing tank. It is shown that the distribution of observed autocorrelation coefficients is well predicted by a Gaussian random process once the autocorrelation bias has been removed.

## 1. Introduction

Backscatter autocorrelation is the fundamental measurement in pulse-to-pulse coherent Doppler sonar (Garbini et al. 1982; Lhermitte and Serafin 1984). While velocity is determined from the phase of the complex autocorrelation coefficient, the coefficient magnitude is often used as a measure of data quality. Corresponding to each velocity measurement, many commercially available instruments provide a measure of autocorrelation, for example, as a coefficient between 0% and 100%. Recommended minimum values for the autocorrelation coefficient assist the user in collecting high-quality measurements and diagnosing instrumentation problems when necessary. In addition to qualitative assessment, autocorrelation can also provide quantitative information on the expected magnitude of measurement errors. For example, pulse-to-pulse autocorrelation has been used to identify and replace spurious Doppler velocimeter measurements in the surf zone (Elgar et al. 2005). Also, the relationship between velocity measurement error and autocorrelation has been determined through laboratory testing of a coherent Doppler sonar (Zedel et al. 1996).

For a sequence  $\{z_n\}$  of complex-valued backscatter samples, the autocorrelation at a lag of  $k$  pulse-to-pulse intervals is

$$R(k\tau) = E(z_n^* z_{n+k}), \quad (1)$$

where  $E$  denotes expected value,  $*$  denotes complex conjugation, and  $\tau$  is the time interval between successive acoustic transmissions. The autocorrelation coefficient is defined as

$$\rho = \frac{|R(\tau)|}{|R(0)|} = \frac{1}{\sigma^2} |E(z_n^* z_{n+1})|, \quad (2)$$

where  $\sigma^2$  is the variance of the sequence  $\{z_n\}$ . By definition,  $\rho$  is a number between zero and one that expresses the degree of pulse-to-pulse autocorrelation.

In practice, autocorrelation is estimated from a finite sequence  $z_1, \dots, z_M$  corresponding to an ensemble of  $M$  pulses (Zrnić 1977),

$$\hat{R}(\tau) = \frac{1}{M-1} \sum_{n=1}^{M-1} z_n^* z_{n+1}. \quad (3)$$

Zedel et al. (1996) define the following autocorrelation coefficient as an estimate of  $\rho$ :

$$\hat{\rho} = \frac{\left| \sum_{n=1}^{M-1} z_n^* z_{n+1} \right|}{\sum_{n=1}^{M-1} |z_n^* z_{n+1}|}. \quad (4)$$

Corresponding author address: Jeremy Dillon, Memorial University of Newfoundland, St. John's NL A1C 5S7, Canada.  
E-mail: jeremy.dillon@mun.ca

The above expression has the desirable property that  $\hat{\rho}$  is a number between zero and one. Also, the numerator resembles (2) in the sense that expected value has been replaced with a finite sum.

For applications in sediment transport, current measurement, and medical ultrasound, scatterers consist of a large number of particles. Each backscatter sample  $z$  is therefore well described by a complex Gaussian distribution, that is,  $z = x + iy$ , where  $x$  and  $y$  are independent normally distributed random variables with equal variances. In general, a time series of backscatter samples is a nonstationary random process because Doppler frequency, autocorrelation, and amplitude are functions of time. However, in the analysis of coherent Doppler systems, backscatter samples are frequently modeled as being drawn from a wide-sense stationary (WSS) random process with Gaussian power spectral density (Garbini et al. 1982; Lhermitte and Serafin 1984; Zedel et al. 1996),

$$P_{zz} = \frac{\sigma^2}{\sigma_f \sqrt{2\pi}} e^{-(f-f_D)^2/2\sigma_f^2}, \quad (5)$$

where  $f_D$  is the mean Doppler frequency and  $\sigma_f$  denotes the spectral width. In this article, the term ‘‘Gaussian distribution’’ refers to the probability distribution of a single backscatter sample. The term ‘‘Gaussian random process’’ refers to a time series where (i) each sample obeys a Gaussian distribution, and (ii) the power spectrum of the time series is a Gaussian function as in (5).

Autocorrelation is determined from the inverse Fourier transform of the power spectral density

$$\begin{aligned} R(t) &= \frac{\sigma^2}{\sigma_f \sqrt{2\pi}} \int_{-\infty}^{\infty} e^{-(f-f_D)^2/2\sigma_f^2} e^{i2\pi ft} df \\ &= \sigma^2 e^{-2\pi^2 \sigma_f^2 t^2} e^{i2\pi f_D t}. \end{aligned} \quad (6)$$

At an autocorrelation lag of one pulse-to-pulse interval, the autocorrelation coefficient  $\rho$  is

$$\rho = \frac{|R(\tau)|}{R(0)} = e^{-2\pi^2 \sigma_f^2 \tau^2}. \quad (7)$$

Therefore,  $\rho$  determines the width of the Doppler spectrum, and hence the variance of velocity measurements.

To compare coherent Doppler sonar observations with expected performance based on a Gaussian random process, it is necessary to examine the relationship between the true autocorrelation coefficient  $\rho$  and its estimate  $\hat{\rho}$ . As increasingly more pulse pairs are averaged, one would expect the accuracy of the autocorrelation estimate to improve. Nevertheless, it is shown in this article that  $\hat{\rho}$  is a biased estimator both for finite averages

and in the limit of infinite ensemble length. However, the relationship between  $\hat{\rho}$  and  $\rho$  may be inverted to obtain unbiased estimates of autocorrelation from biased samples of  $\hat{\rho}$ . The results presented in this article allow theoretical predictions of velocity variance, such as those in Zrnić (1977), to be expressed in terms of the observed autocorrelation estimate rather than the true (but typically unknown) autocorrelation  $\rho$ . Because the effectiveness of pulse-pair averaging depends on the correlation between successive measurements, a sonar designer may wish to know how much averaging is required to sufficiently attenuate measurement errors for a given observed coefficient  $\hat{\rho}$ .

This article is organized as follows. In section 2, a new formula is presented for the asymptotic estimator  $\hat{\rho}_\infty = \lim_{M \rightarrow \infty} \hat{\rho}$ . In section 3, properties of  $\hat{\rho}$  are determined for finite pulse-pair averages via numerical simulation. Sections 4 and 5 describe the apparatus and methods employed in a towing tank experiment. Experimental results appear in section 6, followed by a discussion in section 7. Our conclusions are summarized in section 8.

## 2. Theory

The autocorrelation coefficient in (4) may be written as

$$\hat{\rho} = \frac{\left| \frac{1}{M-1} \sum_{n=1}^{M-1} z_n^* z_{n+1} \right|}{\frac{1}{M-1} \sum_{n=1}^{M-1} |z_n| |z_{n+1}|}. \quad (8)$$

As  $M \rightarrow \infty$ , the numerator converges to  $|R(\tau)| = \rho \sigma^2$ . Assuming that each sample  $z_n$  is described by a Gaussian distribution, the denominator converges to the mean  $\mu$  of the product of two dependent Rayleigh random variables  $|z_n|$  and  $|z_{n+1}|$ . The product  $|z_n| |z_{n+1}|$  is described by the probability distribution (Simon 2002, chapter 6)

$$p(r) = \frac{4r}{\sigma^4(1-\rho^2)} K_0 \left[ \frac{2r}{\sigma^2(1-\rho^2)} \right] I_0 \left[ \frac{2r\rho}{\sigma^2(1-\rho^2)} \right], \quad (9)$$

where  $r = |z_n| |z_{n+1}|$ ,  $K_0$  is a modified Bessel function of the second kind, and  $I_0$  is a modified Bessel function of the first kind. The mean  $\mu$  is determined from

$$\begin{aligned} \mu &= \int_0^\infty rp(r) dr \\ &= \frac{4}{\sigma^4(1-\rho^2)} \int_0^\infty r^2 K_0 \left[ \frac{2r}{\sigma^2(1-\rho^2)} \right] I_0 \left[ \frac{2r\rho}{\sigma^2(1-\rho^2)} \right] dr. \end{aligned} \quad (10)$$

In the appendix, the integral is evaluated in terms of the complete elliptic integral of the second kind  $\mathbf{E}(k)$ ,

$$\mu = \frac{\sigma^2(1+\rho)}{2} \mathbf{E} \left( \frac{2\sqrt{\rho}}{1+\rho} \right). \quad (11)$$

The asymptotic estimate is, therefore,

$$\hat{\rho}_\infty = \frac{\rho\sigma^2}{\mu} = \frac{2\rho}{(1+\rho)\mathbf{E} \left( \frac{2\sqrt{\rho}}{1+\rho} \right)}. \quad (12)$$

For small values of  $\rho$ , the first-order Taylor series is

$$\hat{\rho}_\infty \approx \frac{4\rho}{\pi} \text{ as } \rho \rightarrow 0. \quad (13)$$

For values of  $\rho$  near one, the first-order Taylor series is given by

$$\hat{\rho}_\infty \approx \frac{\rho+1}{2} \text{ as } \rho \rightarrow 1. \quad (14)$$

The asymptotic estimate and asymptotic ratio  $\hat{\rho}_\infty/\rho$  are plotted in Figs. 1a,b, respectively. It is evident that the asymptotic estimate is biased for  $\rho < 1$ .

### 3. Numerical simulation

#### a. Gaussian random process

Numerical simulations of a complex Gaussian process were performed using the MATLAB randn generator. Let  $\zeta_1, \dots, \zeta_M$  denote an ensemble of  $M$  independent identically distributed samples from a complex Gaussian distribution with zero mean and unit variance. For a Gaussian power spectrum, the backscatter autocorrelation sequence  $R_k$  is given by (6) and (7),

$$R_k = \sigma^2 \rho^{k^2} e^{i2\pi f_D \tau k}. \quad (15)$$

Let  $\mathbf{z}$  denote samples  $z_1, \dots, z_M$  arranged as a vector. The corresponding covariance matrix  $\mathbf{C}_z$  is given by (Kay 1993, chapter 15)

$$\mathbf{C}_z = \begin{bmatrix} R_0 & R_{-1} & \cdots & R_{-(M-1)} \\ R_1 & R_0 & \cdots & R_{-(M-2)} \\ \vdots & \vdots & \ddots & \vdots \\ R_{M-1} & R_{M-2} & \cdots & R_0 \end{bmatrix}. \quad (16)$$

By definition,  $\mathbf{C}_z$  is Hermitian positive definite and therefore can be written in terms of the Cholesky decomposition (Watkins 2002, chapter 1)

$$\mathbf{C}_z = \mathbf{U}^* \mathbf{U}. \quad (17)$$

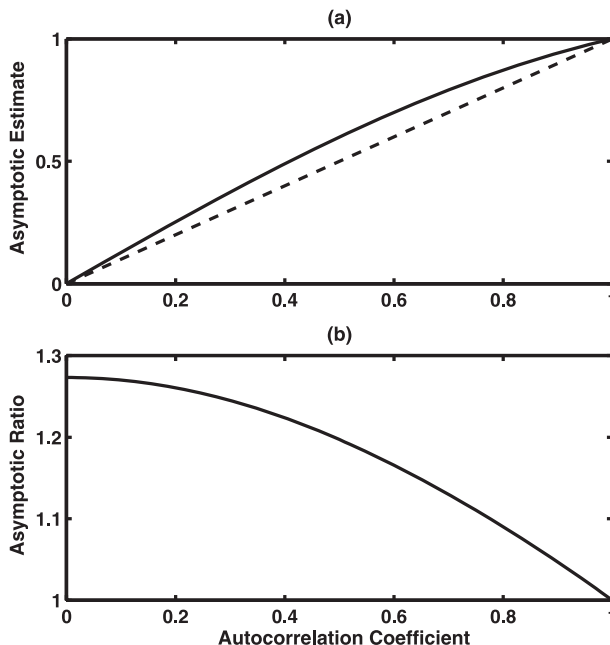


FIG. 1. Asymptotic autocorrelation estimate  $\hat{\rho}_\infty$  from (12) as a function of the actual autocorrelation coefficient  $\rho$ . (a) The ideal relation  $\hat{\rho}_\infty = \rho$  is represented (dashed line). In (b), the ratio  $\hat{\rho}_\infty/\rho$  is displayed.

Here,  $\mathbf{U}$  is an upper triangular matrix with positive diagonal entries and  $\mathbf{U}^*$  denotes the conjugate transpose of  $\mathbf{U}$ . The vector  $\boldsymbol{\zeta}$  of independent samples  $\zeta_1, \dots, \zeta_M$  has covariance matrix  $E(\boldsymbol{\zeta}\boldsymbol{\zeta}^*) = \mathbf{I}$ . Simulated backscatter samples were generated using the transformation

$$\mathbf{z} = \mathbf{U}^* \boldsymbol{\zeta}. \quad (18)$$

Therefore,  $\mathbf{z}$  has covariance matrix given by

$$E(\mathbf{z}\mathbf{z}^*) = E(\mathbf{U}^* \boldsymbol{\zeta} \boldsymbol{\zeta}^* \mathbf{U}) = \mathbf{U}^* E(\boldsymbol{\zeta}\boldsymbol{\zeta}^*) \mathbf{U} = \mathbf{C}_z \quad (19)$$

as desired.

Samples of the autocorrelation estimate  $\hat{\rho}$  were generated from  $10^7$  simulated pings for ensemble lengths of  $M = 10, 20, 40,$  and  $100$ , and true autocorrelation coefficients ranging from  $0.2$  to  $0.98$  in increments of  $0.02$ . For each pair  $(\rho, M)$ , the mean autocorrelation estimate was calculated as an approximation to the expected value  $E(\hat{\rho})$ . The ratio  $E(\hat{\rho})/\rho$  is plotted in Fig. 2, where the dashed line is the asymptotic ratio  $\hat{\rho}_\infty/\rho$  from (12). Although the asymptotic ratio is only strictly valid for  $M \rightarrow \infty$ , simulations for larger values of  $M$  indicated that in the interval of  $\rho \geq 0.2$ , the autocorrelation ratio is within 1% of the asymptotic ratio when  $M$  is greater than or equal to 600.

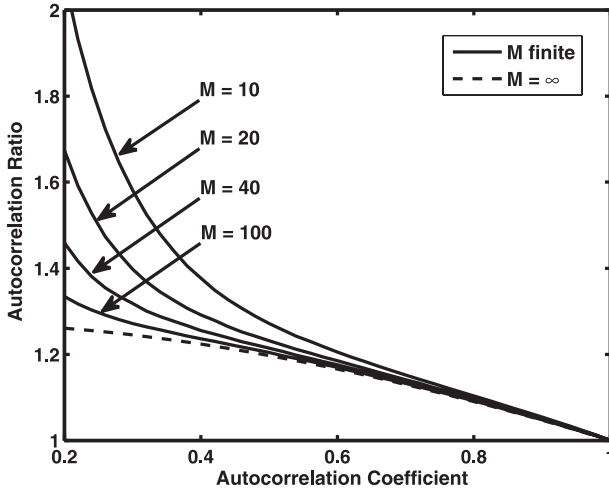


FIG. 2. Estimated autocorrelation coefficients from simulation of a Gaussian random process. Each curve represents the ratio  $E(\hat{\rho})/\rho$  plotted as a function of the true autocorrelation coefficient  $\rho$  for a fixed ensemble length  $M$ . The dashed line is the asymptotic ratio  $\hat{\rho}_\infty/\rho$  from (12).

*b. Coherent Doppler sonar model*

Numerical simulation of steady flow was also performed with the coherent Doppler sonar model described in Zedel (2008). The model simulates pulse-to-pulse coherent scattering from a cloud of moving particles for arbitrary multistatic sonar geometries. Physical effects such as spherical spreading, acoustic absorption, frequency-dependent beam patterns, transducer frequency response, and receiver noise are included in the model. The model supports simulation of arbitrary pulse shapes, including the use of multiple carrier frequencies.

Simulations were performed for a monostatic sonar measuring horizontal velocities of 0.5, 1.5, 3.0, and 4.5 m s<sup>-1</sup>. In the model, the sonar was tilted 5° from vertical to reproduce the geometry of the towing tank experiment described in section 4. Parameters for the coherent Doppler sonar simulation are listed in Tables 1 and 2.

The model was configured to record the result from each ping in addition to calculating pulse-pair averages. The true autocorrelation coefficient was approximated by averaging over all simulated pings,

$$\rho \approx \frac{1}{\sigma^2} \left| \frac{1}{N-1} \sum_{n=1}^{N-1} z_n^* z_{n+1} \right|, \quad (20)$$

where  $\sigma^2$  is the variance of the backscatter sequence  $\{z_n\}$  and  $N = 2 \times 10^5$  is the total number of simulated pings. The mean autocorrelation estimate  $E(\hat{\rho})$  was calculated for ensemble lengths of  $M = 10, 20, 40, 100,$

TABLE 1. Coherent Doppler sonar parameters.

Parameter	Value
Transducer center frequency	1.7 MHz
Transducer bandwidth	1.0 MHz
Receiver bandwidth	250 kHz
Carrier frequency	1.8 MHz
Transmit pulse length	4 $\mu$ s
Ping interval	1.5 ms
Transducer diameter	2 cm

and 1000. Figure 3 shows the ratio  $E(\hat{\rho})/\rho$  corresponding to each velocity. As  $M$  is increased, the ratio converges toward the asymptotic ratio  $\hat{\rho}_\infty/\rho$  specified by (12).

**4. Apparatus**

A towing tank experiment was performed using the multifrequency coherent Doppler sonar described in Hay et al. (2008). Each circular piezocomposite transducer has a diameter of 2 cm, a nominal center frequency of 1.7 MHz, and a bandwidth of approximately 1 MHz. Carrier frequencies, profiling range, range resolution, pulse length, pulse-to-pulse interval, and ensemble length are configurable in software. The dimensions of each sample volume are determined by the beam pattern, carrier frequency, and range resolution. Nominally, each sample point has a diameter of 2 cm and a height of 3 mm. The parameters in Table 1 also apply for the sonar used in the towing tank experiment.

The experiment was performed in the Marine Craft Model Towing Tank at Dalhousie University. The tank has horizontal dimensions of 30 m  $\times$  1 m and a depth of 1 m. An instrumented carriage is propelled by an electric motor along rails mounted above the tank. Carriage speed is computer controlled and programmable over a range from 0 to 3.0 m s<sup>-1</sup>. Constant speed is sustained over a rail length of approximately 25 m. The towing carriage and instrumentation are shown schematically in Fig. 4. The sonar was rotated to point 5° aft (i.e., counterclockwise in Fig. 4) to avoid receiving multiple reflections from the tank bottom. The sonar was located on the tank center line with the center transducer 56 cm

TABLE 2. Parameters for the coherent Doppler sonar simulation.

Parameter	Value
Particle density	4720 L <sup>-1</sup>
Receiver signal-to-noise ratio	10 dB
Simulation time step	12.5 ns
Simulation time	300 s

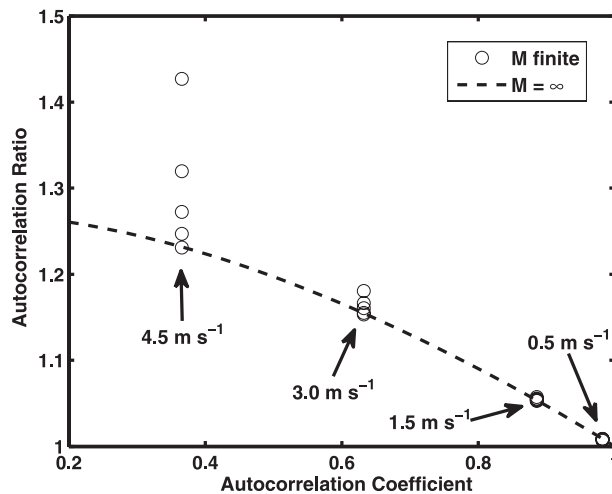


FIG. 3. Estimated autocorrelation coefficients from the coherent Doppler sonar simulation. Each circle represents the ratio  $E(\hat{\rho})/\rho$  plotted as a function of the true autocorrelation coefficient  $\rho$  for ensemble lengths of  $M = 10, 20, 40, 100,$  and  $1000$ . The asymptotic ratio  $\hat{\rho}_\infty/\rho$  from (12) is shown (dashed line). For increasing values of  $M$ , circles converge downward to the dashed line.

above the bottom. Water in the tank was seeded with agricultural lime. Prior to each run, approximately 0.5 kg of lime was added to replace scatterers lost to settling. A rough estimate of sediment concentration was  $1 \text{ g L}^{-1}$ .

## 5. Experimental procedure

Carriage speed was varied from 0.05 to  $3.0 \text{ m s}^{-1}$  by programming the desired speed into the towing tank control system. Results are presented in section 6 for velocities of 0.5, 1.5, and  $3.0 \text{ m s}^{-1}$ . The control system software automatically calculated an acceleration and deceleration profile to maximize the time at constant speed subject to the tank length constraint. Two runs were performed for each speed with a duration of 55 s, or the time elapsed in traversing the entire tank length, whichever was less. Carriage speed was recorded by the control system.

Autocorrelation coefficients were recorded by the sonar data acquisition system using a fixed ensemble length of  $M = 10$ . Because it was not possible to simultaneously record data with multiple ensemble lengths, an indirect approach was taken to assess the validity of simulations in section 3. For each carriage speed, the  $M = 10$  curve from Fig. 2 was used to infer the true autocorrelation coefficient  $\rho$  from the mean of the observed estimates  $\hat{\rho}$ . Histograms of towing tank autocorrelation coefficients were compared with those from a Gaussian random process, as described in section 6.

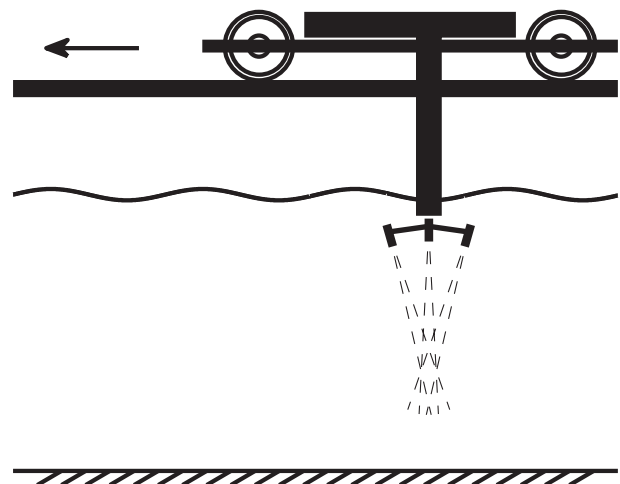


FIG. 4. Side view schematic of the towing tank showing the multifrequency coherent Doppler sonar. Instrumentation was attached to a carriage that moved along rails mounted above the water. Transducer beam patterns are indicated (dashed lines).

## 6. Results

In Table 3, the mean autocorrelation estimate  $E(\hat{\rho})$  was calculated for towing carriage speeds of 0.5, 1.5, and  $3.0 \text{ m s}^{-1}$  from the 41-cm range bin of the center transducer receiver channel. Here,  $E(\hat{\rho})$  represents the mean magnitude of observed autocorrelation coefficients, which is similar to the measure of data quality reported by commercial instruments. Table 3 also lists the corresponding true autocorrelation coefficients estimated from the  $M = 10$  curve in Fig. 2. These values of  $\rho$  were used to generate autocorrelation coefficients from a Gaussian random process, as described in section 3.

Distributions of towing tank autocorrelation coefficients are shown in Fig. 5 for carriage speeds of 0.5, 1.5, and  $3.0 \text{ m s}^{-1}$ . Values of  $\hat{\rho}$  from the center transducer receiver channel were grouped in 30 equally spaced bins and plotted as histograms. Dotted lines in Fig. 5 represent distributions of  $\hat{\rho}$  from a Gaussian random process with  $M = 10$  and  $\rho$  as listed in Table 3. Dashed lines in Fig. 5 represent distributions of  $\hat{\rho}$  that result from assuming that no bias exists, that is, that  $\rho \approx E(\hat{\rho})$ . Histograms were generated from  $10^7$  simulated

TABLE 3. Estimated autocorrelation coefficients from towing tank data.

Velocity ( $\text{m s}^{-1}$ )	$E(\hat{\rho})$	$\rho$ from Fig. 2
0.5	0.990	0.977
1.5	0.948	0.899
3.0	0.817	0.713

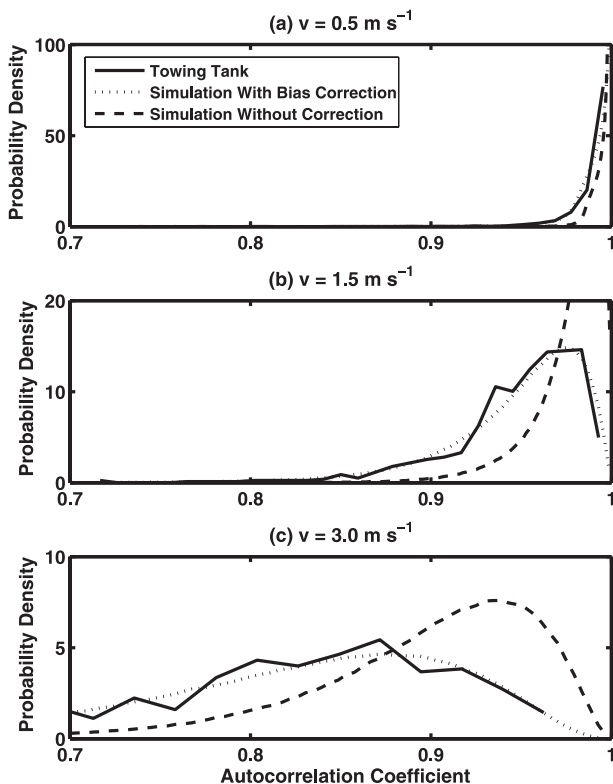


FIG. 5. Distributions of measured and simulated autocorrelation coefficients. A histogram of  $\hat{\rho}$  from the 41-cm range bin of the center transducer 1.8-MHz receiver channel (solid lines). The corresponding distributions from a Gaussian random process where the autocorrelation bias has been removed using the  $M = 10$  curve in Fig. 2 are also shown (dotted lines). Simulated distributions with no bias correction are represented (dashed lines). Carriage speed is (top) 0.5 and (bottom) 3.0  $\text{m s}^{-1}$ .

pings, with autocorrelation coefficients grouped in 200 equally spaced bins.

### 7. Discussion

The derivation of the asymptotic autocorrelation coefficient assumed a complex Gaussian probability distribution for each backscatter sample. However, it was not necessary to assume a Gaussian power spectrum for the time series because the asymptotic formula depends only on the expected autocorrelation at a lag of one pulse-to-pulse interval. The formula was presented in terms of an elliptic integral. Although  $\mathbf{E}(k)$  cannot be expressed in terms of elementary functions, it may be evaluated numerically, for example, with the ellipke function in MATLAB.

Numerical simulation of a Gaussian random process showed that the bias of the autocorrelation coefficient increases for short ensemble lengths. For example, the

degenerate case of a single pulse pair results in a coefficient of one regardless of the actual pulse-to-pulse autocorrelation. A longer ensemble length is necessary to obtain meaningful autocorrelation estimates. As shown in Fig. 2, a bias persists for all of the ensemble lengths, with convergence to the asymptotic formula occurring for  $M$  approximately equal to 600. The bias is more significant for small values of the autocorrelation coefficient. For practical applications where reasonably high-quality data are obtained (say  $\rho \geq 0.7$ ), there is negligible variation in the ratio  $\hat{\rho}/\rho$  as  $M$  is varied. However, a bias is still present for  $\rho \geq 0.7$ , and in this case the bias is well described by the asymptotic Eq. (12).

The coherent Doppler sonar model in Zedel (2008) does not require any Gaussian assumption about the backscatter probability distribution or the time series power spectrum. The model describes the physics of coherent scattering and accounts for the sonar geometry and operating parameters, unlike the simulations of a Gaussian random process in section 3. Simulations of steady flow confirmed that the autocorrelation coefficient converges to the asymptotic formula as ensemble length is increased. However, similarity between Figs. 2 and 3 shows that simulation of a Gaussian random process is sufficient to predict the bias of the autocorrelation coefficient.

In Table 3, the mean observed autocorrelation estimates from the towing tank satisfy  $E(\hat{\rho}) > 0.8$ , which is within the range of acceptable data quality for commercial instruments. Although the towing tank experiment was performed for a single ensemble length, results in Fig. 5 validate the relationship between  $\hat{\rho}$  and  $\rho$  for the  $M = 10$  curve in Fig. 2. When it is assumed that  $\rho \approx E(\hat{\rho})$ , instead of accounting for the autocorrelation bias, simulated histograms in Fig. 5 do not match experimental observations. As expected, the discrepancy increased with velocity due to backscatter decorrelation from particle advection through the sonar sample volume. However, when the autocorrelation bias is removed, simulated distributions of the autocorrelation coefficient closely match experimental observations. The towing tank experiment confirms the validity of the Gaussian random process for predicting the bias of the autocorrelation coefficient. One would therefore expect towing tank observations to converge to the asymptotic formula as the ensemble length is increased.

It would be interesting to repeat the towing tank experiment with additional runs for each carriage speed while recording the result from each ping. Autocorrelation coefficients could be calculated for a range of ensemble lengths to demonstrate convergence to the asymptotic formula, as in section 3, for the coherent Doppler sonar simulation. Reproduction of Fig. 3 with experimental

measurements would require approximately 300 s of data for each speed. At 3.0 m s<sup>-1</sup>, the carriage would need to travel 900 m, requiring 36 runs in the Dalhousie University towing tank. For such an endeavor, a longer tank or a continuously operated flume would be more suitable.

Finally, we remark that the definition of the autocorrelation coefficient is not unique. The coefficient considered in this article is an appropriate choice because 0 ≤  $\hat{\rho}$  ≤ 1 and the numerator  $\sum z_n^* z_{n+1}$  is similar in form to the expected value in the definition of autocorrelation. However, any power or root of  $\hat{\rho}$  also provides a measure of pulse-to-pulse autocorrelation while taking values in the interval [0, 1]. The method presented in the appendix could be applied to analyze the asymptotic behavior of other coefficients. If the analysis turns out to be intractable, one may resort to numerical simulation as in section 3.

**8. Conclusions**

A new formula has been presented for the asymptotic form of an autocorrelation coefficient for coherent Doppler sonar. The derivation showed that the autocorrelation coefficient is a biased estimator in the limit of infinite ensemble length. Numerical simulation of a Gaussian random process indicated that the bias persists for finite pulse-pair averages. Furthermore, the bias increases for shorter ensemble lengths. Validity of the Gaussian random process was confirmed with numerical simulation using a high-fidelity coherent Doppler sonar model, and from sonar measurements in a towing tank where the towing carriage traveled at constant speed. The experiment showed that the distribution of observed autocorrelation coefficients is well predicted by a Gaussian random process once the autocorrelation bias has been removed. Although other autocorrelation coefficients may be defined, the analysis and numerical methods developed in this article could be applied to derive their asymptotic behavior.

*Acknowledgments.* We thank Richard Cheel for experimental support and Robert Craig for data acquisition software. Financial support for J. Dillon was provided by the Link Foundation and the Natural Sciences and Engineering Research Council of Canada.

APPENDIX

**Derivation of the Asymptotic Coefficient**

In section 2, the asymptotic autocorrelation coefficient was shown to be

$$\hat{\rho}_\infty = \frac{\rho\sigma^2}{\mu}, \tag{A1}$$

where the denominator  $\mu$  is given by

$$\mu = \frac{4}{\sigma^4(1-\rho^2)} \int_0^\infty r^2 K_0\left[\frac{2r}{\sigma^2(1-\rho^2)}\right] I_0\left[\frac{2r\rho}{\sigma^2(1-\rho^2)}\right] dr. \tag{A2}$$

The following identity results from the integral 6.576–5 of Gradshteyn and Ryzhik (2007):

$$\int_0^\infty r^2 K_0(ar) I_0(br) dr = \frac{2\Gamma\left(\frac{3}{2}\right)^2}{a^3\Gamma(1)} F\left(\frac{3}{2}, \frac{3}{2}; 1; \frac{b^2}{a^2}\right), \tag{A3}$$

where  $\Gamma(z) = \int_0^\infty t^{z-1} e^{-t} dt$  is the gamma function and  $F$  is the hypergeometric function (Ahlfors 1966, chapter 8). Equation (A3) is valid when  $a > b$ . The gamma function satisfies  $\Gamma(1) = 1$  and  $\Gamma(3/2) = \sqrt{\pi}/2$ , resulting in

$$\int_0^\infty r^2 K_0(ar) I_0(br) dr = \frac{\pi}{2a^3} F\left(\frac{3}{2}, \frac{3}{2}; 1; \frac{b^2}{a^2}\right). \tag{A4}$$

To apply (A4) to (A2), let

$$a = \frac{2}{\sigma^2(1-\rho^2)}, \tag{A5}$$

$$b = \frac{2\rho}{\sigma^2(1-\rho^2)}. \tag{A6}$$

Therefore,  $b/a = \rho$  implies that  $a > b$  is satisfied when  $\rho < 1$ . Equation (A4) becomes

$$\int_0^\infty r^2 K_0(ar) I_0(br) dr = \frac{\pi\sigma^6(1-\rho^2)^3}{16} F\left(\frac{3}{2}, \frac{3}{2}; 1; \rho^2\right). \tag{A7}$$

Substitution of (A7) in (A2) results in

$$\mu = \frac{\pi\sigma^2(1-\rho^2)^2}{4} F\left(\frac{3}{2}, \frac{3}{2}; 1; \rho^2\right). \tag{A8}$$

The integral 9.112 of Gradshteyn and Ryzhik (2007) may be used to evaluate the hypergeometric function,

$$F\left(\frac{3}{2}, \frac{3}{2}; 1; \rho^2\right) = \frac{1}{2\pi} \int_0^{2\pi} \frac{dx}{(1+\rho^2-2\rho\cos x)^{3/2}}. \tag{A9}$$

The following identity appears as integral 2.575–4 in Gradshteyn and Ryzhik (2007):

$$\int \frac{dx}{(c-d \cos x)^{3/2}} = \frac{2}{(c-d)\sqrt{c+d}} \varepsilon(\delta, r), \tag{A10}$$

where

$$\varepsilon(\varphi, k) = \int_0^\varphi \sqrt{1-k^2 \sin^2 x} dx \tag{A11}$$

is the elliptic integral of the second kind, and

$$\delta = \sin^{-1} \sqrt{\frac{(c+d)(1-\cos x)}{2(c-d \cos x)}}, \tag{A12}$$

$$r = \sqrt{\frac{2d}{c+d}}. \tag{A13}$$

Equation (A10) is valid for  $c > d > 0$  and  $0 \leq x \leq \pi$ . To apply (A10) to (A9), let

$$c = 1 + \rho^2, \tag{A14}$$

$$d = 2\rho. \tag{A15}$$

Therefore,  $c > d > 0$  is satisfied when  $\rho < 1$ . The parameter  $r$  is given by

$$r = \frac{2\sqrt{\rho}}{1+\rho}. \tag{A16}$$

Symmetry of the integrand in (A9) implies that

$$F\left(\frac{3}{2}, \frac{3}{2}; 1; \rho^2\right) = \frac{1}{\pi} \int_0^\pi \frac{dx}{(1+\rho^2-2\rho \cos x)^{3/2}}. \tag{A17}$$

Because integration occurs over the interval  $0 \leq x \leq \pi$ , (A10) may be used to obtain

$$F\left(\frac{3}{2}, \frac{3}{2}; 1; \rho^2\right) = \frac{2}{\pi(1-\rho)^2(1+\rho)} \varepsilon\left(\delta, \frac{2\sqrt{\rho}}{1+\rho}\right) \Bigg|_0^\pi. \tag{A18}$$

Noting that  $\delta(0) = 0$ ,  $\delta(\pi) = \pi/2$ , and  $\varepsilon(0, k) = 0$ , (A18) reduces to

$$F\left(\frac{3}{2}, \frac{3}{2}; 1; \rho^2\right) = \frac{2}{\pi(1-\rho)^2(1+\rho)} \mathbf{E}\left(\frac{2\sqrt{\rho}}{1+\rho}\right), \tag{A19}$$

where  $\mathbf{E}(k) = \varepsilon(\pi/2, k)$  is the complete elliptic integral of the second kind. Combining (A8) and (A19) results in

$$\mu = \frac{\sigma^2(1+\rho)}{2} \mathbf{E}\left(\frac{2\sqrt{\rho}}{1+\rho}\right). \tag{A20}$$

Substitution of (A20) in (A1) produces the final result,

$$\hat{\rho}_\infty = \frac{2\rho}{(1+\rho)\mathbf{E}\left(\frac{2\sqrt{\rho}}{1+\rho}\right)}. \tag{A21}$$

REFERENCES

Ahlfors, L. V., 1966: *Complex Analysis*. 2nd ed. McGraw-Hill, 317 pp.

Elgar, S., B. Raubenheimer, and R. T. Guza, 2005: Quality control of acoustic Doppler velocimeter data in the surfzone. *Meas. Sci. Technol.*, **16**, 1889–1893.

Garbini, J. L., F. K. Forster, and J. E. Jorgensen, 1982: Measurement of fluid turbulence based on pulsed ultrasound techniques. Part 1. Analysis. *J. Fluid Mech.*, **118**, 445–470.

Gradshteyn, I. S., and I. M. Ryzhik, 2007: *Tables of Integrals, Series, and Products*. 7th ed. Academic Press, 1200 pp.

Hay, A. E., L. Zedel, R. Craig, and W. Paul, 2008: Multi-frequency, pulse-to-pulse coherent Doppler sonar profiler. *Proc. IEEE/OES Ninth Working Conf. on Current Measurement Technology*, Charleston, SC, IEEE, 25–29.

Kay, S. M., 1993: *Fundamentals of Statistical Signal Processing: Estimation Theory*. Vol. 1. Prentice-Hall PTR, 625 pp.

Lhermitte, R., and R. Serafin, 1984: Pulse-to-pulse coherent Doppler sonar signal processing techniques. *J. Atmos. Oceanic Technol.*, **1**, 293–308.

Simon, M. K., 2002: *Probability Distributions Involving Gaussian Random Variables: A Handbook for Engineers and Scientists*. Springer, 232 pp.

Watkins, D. S., 2002: *Fundamentals of Matrix Computations*. 2nd ed. John Wiley & Sons, 640 pp.

Zedel, L., 2008: Modeling pulse-to-pulse coherent Doppler sonar. *J. Atmos. Oceanic Technol.*, **25**, 1834–1844.

—, A. E. Hay, R. Cabrera, and A. Lohrmann, 1996: Performance of a single-beam pulse-to-pulse coherent Doppler profiler. *IEEE J. Oceanic Eng.*, **21**, 290–297.

Zrnić, D. S., 1977: Spectral moment estimates from correlated pulse pairs. *IEEE Trans. Aerosp. Electron. Syst.*, **AES-13**, 344–354.